Journal of Catalysis **192,** 137–148 (2000)
doi:10.1006/jcat.2000.2831, available online at http://www.idealibrary.com on IDEAL®

Selective Reduction of NO with Propene over Ga_2O_3–Al_2O_3: Effect of Sol–Gel Method on the Catalytic Performance

Masaaki Haneda,[1] Yoshiaki Kintaichi, Hiromichi Shimada, and Hideaki Hamada

National Institute of Materials and Chemical Research, 1-1 Higashi, Tsukuba, Ibaraki 305-8565, Japan

Received September 29, 1999; revised January 21, 2000; accepted January 25, 2000

The effect of the preparation method on the activity of Ga_2O_3–Al_2O_3 for the selective reduction of NO with propene was investigated. Ga_2O_3–Al_2O_3 prepared by the sol–gel method (Ga_2O_3–Al_2O_3(S)) exhibited excellent activity for NO reduction, compared with Al_2O_3, Ga_2O_3, and impregnated Ga_2O_3/Al_2O_3 (Ga_2O_3/Al_2O_3(I)). XRD measurements of Ga_2O_3–Al_2O_3(S) indicated that a part of the Al^{3+} ions in Al_2O_3 are substituted by Ga^{3+} ions, resulting in the formation of a composite oxide, $[Ga_xAl_{(1-x)}]_2O_3$ ($x < 1$). On the other hand, Ga_2O_3 particles and Al_2O_3 particles were found to be present separately for Ga_2O_3/Al_2O_3(I). The high catalytic activity of Ga_2O_3–Al_2O_3(S) was accounted for by the high surface area and the nature of the $[Ga_xAl_{(1-x)}]_2O_3$ ($x < 1$) composite oxide, which was formed uniformly by the present sol–gel method. The comparison of the reactivity between NO and NO_2 suggested the participation of NO_2 in NO reduction. The kinetic order for NO reduction was found to be 0.3 with respect to propene and 0.7 with respect to oxygen on both Ga_2O_3/Al_2O_3(I) and Ga_2O_3–Al_2O_3(S). However, a significant difference in the reaction order with respect to NO was observed between Ga_2O_3/Al_2O_3(I) and Ga_2O_3–Al_2O_3(S), 0.4 order on the former catalyst, and zero order on the latter one, indicating the presence of strongly adsorbed NOx species on the catalyst surface. On the basis of these results, a reaction mechanism was proposed in which the NOx adspecies formed through NO oxidation is reduced to nitrogen via organic intermediates containing nitrogen and oxygen.

Key Words: **nitrogen monoxide; selective reduction; propene; Ga_2O_3–Al_2O_3; sol–gel method; kinetic studies.**

1. INTRODUCTION

Selective catalytic reduction of nitrogen oxides (NOx) to N_2 by hydrocarbons has recently received extensive attention because of its potential for practical applications to diesel and lean-burn engine exhausts (1). The principal advantage of this process is its ability to reduce NOx in the presence of oxygen (2, 3) and the easiness of handling hydrocarbons as reductant compared with ammonia which is currently used for NOx removal for stationary engines and boilers.

[1] To whom correspondence should be addressed. Fax: +81-298-54-4487. E-mail: hane@nimc.go.jp.

Since Cu–ZSM-5 was reported as a highly active catalyst by Held *et al.* (4) and Iwamoto *et al.* (5) following earlier patents from Volkswagen (6) and Toyota (7), a lot of investigations have focused on zeolite-based catalysts (8–11). Although metal ion-exchanged zeolites showed excellent activity at high space velocities, their hydrothermal instability due to dealumination from the zeolite framework is a big problem (12, 13).

In addition to zeolite-based catalysts, metal oxide-based catalysts such as single metal oxides (14–17), binary oxides (18), and metal-supported oxides (19–38) have also been found to catalyze the selective reduction of NO with hydrocarbons or oxygenated hydrocarbons. In particular, supported alumina catalysts such as Co/Al_2O_3 (20–22, 26, 33), Sn/Al_2O_3 (23, 25), and Ag/Al_2O_3 (27, 29, 30–32, 34, 35) are regarded as promising candidates for practical applications.

The catalytic activity and selectivity of metal-supported alumina are well known to depend strongly upon the dispersion, loading, and local structure of metal additives. For example, the activity of Co/Al_2O_3, which is one of the catalysts studied most extensively, is affected strongly by the preparation method and the calcination temperature. When Co/Al_2O_3 was prepared by the sol–gel method (21) or was heated at temperature higher than 873 K (21, 22, 26, 33), fairly high catalytic activity was attained. The high activity should be due to highly dispersed cobalt species on alumina. Recently, Yan *et al.* (26) proposed the importance of the coordination number of Co^{2+} ions in $CoAl_2O_4$ and small Co_3O_4 particles as a factor to determine the NO reduction activity. According to their report, dispersed octahedrally coordinated Co^{2+} ions are responsible for the catalytic activity.

Shimizu *et al.* (36, 37) reported interesting catalytic behavior of Ga/Al_2O_3 prepared by the impregnation method for NO reduction by methane. They found that the activity of Ga/Al_2O_3 increased with increasing gallium loading up to about 30 wt%, at which a theoretical monolayer coverage of gallium oxide on alumina is formed. According to their considerations, gallium oxide highly dispersed on alumina is responsible for the high activity and selectivity. The

0021-9517/00 $35.00

preparation method is also presumed to affect the catalytic activity of Ga/Al_2O_3. In fact, we found that Ga_2O_3–Al_2O_3 prepared by the sol–gel method exhibited much higher activity for NO reduction by propene than that prepared by the impregnation method (38). In the present study, we have investigated various factors affecting the catalytic activity of Ga_2O_3–Al_2O_3 for the selective reduction of NO with propene in detail. Several characterization techniques were employed to reveal important factors related to the catalytic activity. We also performed kinetic studies to discuss the mechanistic features of NO reduction on Ga_2O_3–Al_2O_3.

2. EXPERIMENTAL

2.1. Catalyst Preparation

Al_2O_3 was synthesized from aluminum boehmite sol prepared by hydrolysis of aluminum(III) triisopropoxide (AIP) in hot water (363 K) with a small amount of nitric acid (39–41). The sol solution thus obtained was heated under reduced pressure to remove the solvents. The residue was dried at 383 K in an oven and then calcined at 873 K for 5 h in flowing air. Ga_2O_3 was prepared from gallium hydroxide which was obtained by adding urea to an aqueous solution of gallium(III) nitrate and stirring at 363 K for 10 h. The precipitate thus obtained was washed with distilled water, followed by drying at 383 K and calcination at 873 K for 5 h in flowing air.

Ga_2O_3–Al_2O_3 catalysts were prepared by two different methods (abbreviated as Ga_2O_3/Al_2O_3(I) and Ga_2O_3–Al_2O_3(S)). Ga_2O_3/Al_2O_3(I) was prepared by impregnating the above-mentioned alumina with an aqueous solution of gallium(III) nitrate. Ga_2O_3–Al_2O_3(S) was prepared by the sol–gel method. A solution of gallium(III) nitrate dissolved in ethylene glycol was first added into the aluminum boehmite sol solution produced in the manner as described above. After the solution was stirred at room temperature for 1 day, the solvents were eliminated by heating under reduced pressure. The resulting catalyst precursors were dried at 383 K, followed by calcination at 873 K for 5 h in flowing air. Some catalyst samples were further calcined at 1073 and 1273 K for 5 h in air. Basically, the gallium loading for Ga_2O_3/Al_2O_3(I) and Ga_2O_3–Al_2O_3(S) was fixed at 30 wt% as Ga_2O_3, although Ga_2O_3–Al_2O_3(S) with different Ga_2O_3 content from 5 wt% to 70 wt% was also prepared.

2.2. Catalytic Activity Measurements

2.2.1. Evaluation of NO reduction activity. The catalytic activity was measured by using a fixed-bed flow reactor. A feed gas mixture containing nitrogen oxides (900 ppm NO or 930 ppm NO_2), 900 ppm C_3H_6, 10% oxygen, and 0 or 9.1% H_2O diluted in helium as a balance gas was fed to 0.2 g of a catalyst at a rate of 66 cm^3 min^{-1} ($W/F = 0.18$ g scm^{-3}). H_2O was introduced into the reaction gas mixture with a micropump. When H_2O was used, the feed gas flow rate and the concentrations of the other gas components were kept the same by controlling the helium flow rate. The reaction temperature was changed stepwise from 873 to 573 K with a 50 K step. The effluent gas was analyzed by gas chromatogrphy (Shimadzu GC8A TCD). A molecular sieve 5A column was used for the analysis of N_2 and CO and a Porapak Q column for that of N_2O, CO_2, and C_3H_6. The catalytic activity was evaluated in terms of NOx (NO or NO_2) conversion to N_2 and that of propene to COx ($CO + CO_2$). The formation of N_2O was found negligible in the present study.

2.2.2. Kinetic studies. The reaction rate of N_2 formation was measured by changing the catalyst weight from 0.01 to 0.2 g to obtain the conversion of NO in the range of 10–30%. The kinetic parameters were determined at 723 K by assuming the following rate equation:

$$r_{N_2} = k P_{NO}^{\alpha} P_{C_3H_6}^{\beta} P_{O_2}^{\gamma} \exp(-Ea/RT). \quad [1]$$

For this purpose, the concentrations of the reactants were changed in the range of 200–1500 ppm for NO, 200–1500 ppm for C_3H_6, and 3–10% for O_2. The total flow rate was 66 cm^3 min^{-1}. The standard reaction conditions were 900 ppm NO, 900 ppm C_3H_6, and 10% oxygen. The activation energy, E_a in the rate equation [1], was calculated at temperatures ranging from 673 to 773 K under the standard reaction conditions.

2.3. Catalyst Characterization

BET surface area was measured with a conventional flow apparatus (Micromeritics, Flowsorb II 2300) by nitrogen adsorption at 77 K. The nitrogen adsorption isotherm at 77 K was measured volumetrically with a BELSORP 28SA. The pore size distribution curves of the catalyst were calculated, on the basis of Dollimore–Heal (D–H) theory, from the desorption branches of the isotherms. The crystal structure was identified by XRD (Shimadzu XD-D1) measurements using Cu $K\alpha$ radiation at 40 kV and 40 mA. The surface morphology of Ga_2O_3–Al_2O_3 was observed by SEM (Hitachi S-5000) operated at an accelerating voltage of 15 kV. TEM analysis was made with a JEOL JEM-2000FX and at an accelerating voltage of 200 kV.

XPS spectra in the region of Ga 2p and Al 2p were recorded by using a VG Scientific ESCA-5500 with an Mg $K\alpha$ X-ray source ($h\nu = 1253.6$ eV) operated at 15 kV and 20 mA. The binding energy was corrected by the contaminated carbons (284.6 eV). The peak area ratio (Ga 2p/Al 2p) was corrected using relative atomic sensitive factors.

2.4. NO TPD Measurements

Temperature-programmed desorption (TPD) experiments of NOx were carried out by using 50 mg of a sample. The sample was pretreated in a flow of 10% O_2/He at 873 K for 1 h and then cooled to room temperature. NOx adsorption was performed by passing a gas mixture containing 1000 ppm NO and 10% O_2 diluted in He through the sample bed at room temperature for 2 h. After the adsorption gas was purged with He until no NO was detected in the effluent, the TPD measurement was carried out up to 873 K with a heating rate of 5 K min^{-1} in flowing He. The gas flow rate was fixed at 60 cm^3 min^{-1}. The desorbed species with mass numbers of 30 (NO), 32 (O_2), 44 (N_2O), and 46 (NO_2) were monitored continuously by a quadrupole mass spectrometer (ANELVA M-QA200TS) as a function of temperature.

3. RESULTS

3.1. Catalytic Activity of Ga_2O_3–Al_2O_3

3.1.1. Effect of preparation method. Figure 1 compares the catalytic activities of Al_2O_3, Ga_2O_3/Al_2O_3(I), Ga_2O_3–Al_2O_3(S), and Ga_2O_3 for NO reduction by propene in the absence of H_2O. The NO reduction activity of Al_2O_3 was higher than that of Ga_2O_3, although the active temperature region was almost the same. Apparently, the addition of Ga_2O_3 into Al_2O_3 by the impregnation method caused an enhancement of NO conversion. No great difference in propene conversion on these three catalysts was observed. On the other hand, Ga_2O_3–Al_2O_3 prepared by the sol–gel method showed catalytic behavior different from that of the other catalysts. It is obvious that Ga_2O_3–Al_2O_3(S) shows extremely high activity for NO reduction to N_2 in the wide temperature region between 673 and 823 K. Propene conversion on Ga_2O_3–Al_2O_3(S) was also much higher than that on the other catalysts. These results indicate that the preparation method affects strongly the catalytic activity of Ga_2O_3–Al_2O_3.

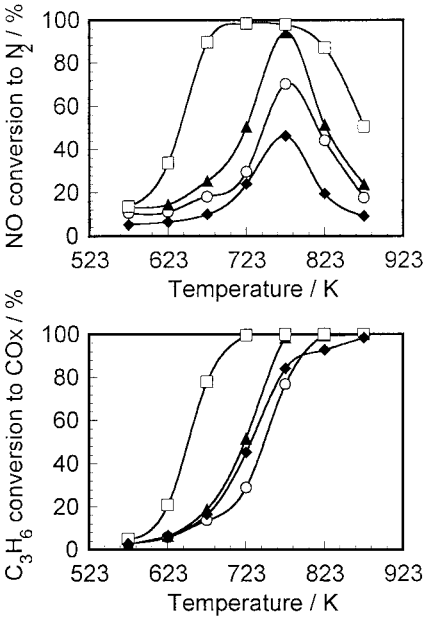

FIG. 1. Catalytic activity of Al_2O_3 (○), Ga_2O_3/Al_2O_3(I) (▲), Ga_2O_3–Al_2O_3(S) (□), and Ga_2O_3 (◆) for the selective reduction of NO with propene in the absence of H_2O. Conditions: NO = 900 ppm, C_3H_6 = 900 ppm, O_2 = 10%, H_2O = 0%, catalyst weight = 0.2 g, W/F = 0.18 g scm^{-3}.

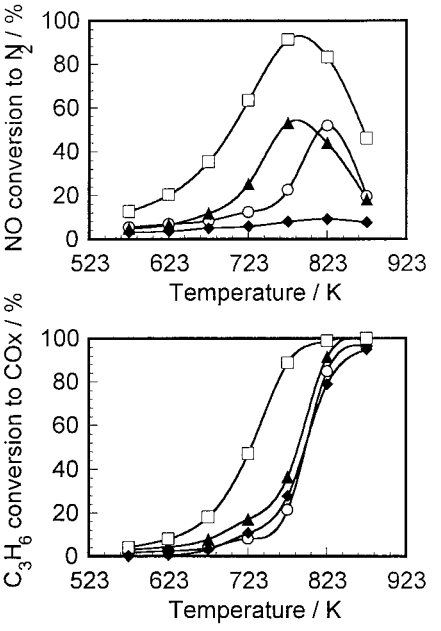

FIG. 2. Catalytic activity of Al_2O_3 (○), Ga_2O_3/Al_2O_3(I) (▲), Ga_2O_3–Al_2O_3(S) (□), and Ga_2O_3 (◆) for the selective reduction of NO with propene in the presence of H_2O. Conditions: NO = 900 ppm, C_3H_6 = 900 ppm, O_2 = 10%, H_2O = 9.1%, catalyst weight = 0.2 g, W/F = 0.18 g scm^{-3}.

Figure 2 shows the catalytic activity of Al_2O_3, Ga_2O_3/Al_2O_3(I), Ga_2O_3–Al_2O_3(S), and Ga_2O_3 for NO reduction by propene in the presence of H_2O. It can be seen by comparing Figs. 1 and 2 that the activity of Ga_2O_3 was depressed considerably by addition of H_2O. Coexisting H_2O was found to decrease the N_2 formation rate over Ga_2O_3 at 723 K by about 20%. Al_2O_3 and Ga_2O_3/Al_2O_3(I) gave almost the same maximum NO conversion with different effective temperatures for NO reduction. Their N_2 formation rate at 723 K in the presence of H_2O was about 30% of that in its absence. Apparently, Ga_2O_3–Al_2O_3(S) showed excellent catalytic performance compared to Al_2O_3, Ga_2O_3/Al_2O_3(I), and Ga_2O_3, although its activity was also decreased by H_2O. In this case, the extent of the decrease of the N_2 formation rate at 723 K by coexisting H_2O was estimated to be about 30%. This means that the tolerances toward H_2O were very similar for Al_2O_3, Ga_2O_3/Al_2O_3(I), and Ga_2O_3–Al_2O_3(S). It was also found that the order of propene conversion on the catalysts is the same irrespective of coexisting H_2O.

The effect of H_2O concentration on the activity of Ga_2O_3–Al_2O_3(S) was examined. The reaction rate for N_2

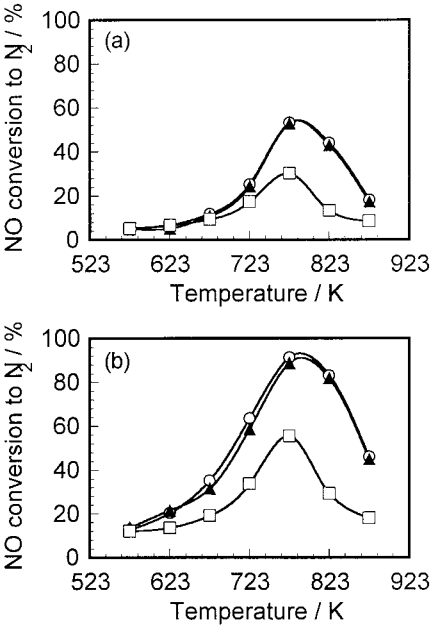

FIG. 3. Effect of calcination temperature on the activity of (a) Ga_2O_3/Al_2O_3(I) and (b) Ga_2O_3–Al_2O_3(S) for NO reduction by propene in the presence of H_2O. The reaction conditions are the same as for Fig. 2. Calcination temperature: (○) 873 K, (▲) 1073 K, and (□) 1273 K.

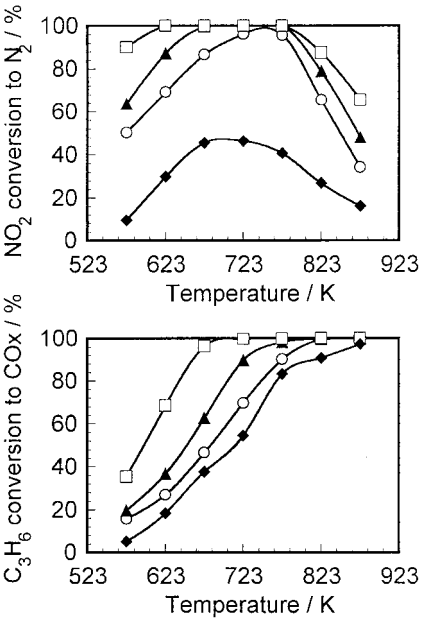

FIG. 4. Catalytic activity of Al_2O_3 (○), Ga_2O_3/Al_2O_3(I) (▲), Ga_2O_3–Al_2O_3(S) (□), and Ga_2O_3 (◆) for the selective reduction of NO_2 with propene in the absence of H_2O. Conditions: $NO_2 = 930$ ppm, $C_3H_6 = 900$ ppm, $O_2 = 10\%$, $H_2O = 0\%$, catalyst weight = 0.2 g, W/F = 0.18 g scm^{-3}.

formation at 723 K decreased with increasing H_2O concentration as follows: 18.6 μmol min^{-1} g^{-1} (H_2O, 0%), 6.81 μmol min^{-1} g^{-1} (H_2O, 0.9%), 5.90 μmol min^{-1} g^{-1} (H_2O, 4.1%), and 5.48 μmol min^{-1} g^{-1} (H_2O, 9.1%). The catalytic performance seems to be affected considerably by the presence of a small amount of H_2O.

3.1.2. Effect of calcination temperature. Figure 3 compares the activity of Ga_2O_3/Al_2O_3(I) and Ga_2O_3-Al_2O_3(S) calcined at 873, 1073, and 1273 K for NO reduction in the presence of H_2O. Obviously, both catalysts showed similar catalytic behavior. No considerable activity depression was observed after the calcination at 1073 K, while the calcination at 1273 K caused a decrease of the activity over the entire temperature range.

3.1.3. Reduction of NO_2 with propene. Figure 4 shows the activities of Al_2O_3, Ga_2O_3/Al_2O_3(I), Ga_2O_3–Al_2O_3(S), and Ga_2O_3 for NO_2 reduction by propene in the absence of H_2O. As can be seen by comparing Fig. 1 with Fig. 4, the replacement of NO with NO_2 resulted in a considerable increase in N_2 formation as well as in COx formation over all the catalysts. The order of NO_2 reduction activity is as follows: $Ga_2O_3 < Al_2O_3 < Ga_2O_3/Al_2O_3$(I) < Ga_2O_3–Al_2O_3(S). This is well consistent with the results for NO reduction, suggesting the participation of NO_2 in NO reduction.

3.1.4. NO oxidation to NO_2. It is well known that NO oxidation into NO_2 is the initial and indispensable step for NO reduction by hydrocarbons over several catalysts (3, 8, 10, 22, 33). Figure 5 shows the activity of Al_2O_3, Ga_2O_3/Al_2O_3(I), Ga_2O_3–Al_2O_3(S), and Ga_2O_3 for NO oxidation to NO_2. Ga_2O_3–Al_2O_3(S) catalyzed most effectively the oxidation of NO by O_2 to NO_2, while Al_2O_3, Ga_2O_3/Al_2O_3(I), and Ga_2O_3 were not effective. This is a quite surprising result because the latter three catalysts catalyzed effectively NO reduction by propene to N_2 but did not catalyze NO oxidation to NO_2. This result seems to contradict the model proposed in which NO oxidation into NO_2 is one of the reaction steps. The low activity for NO oxidation could be explained by the poisoning of the catalyst by NO_2, as suggested in the case of Ag/Al_2O_3 (29) and Co/Al_2O_3

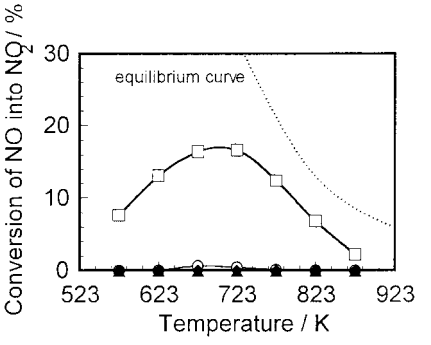

FIG. 5. Catalytic activity of Al_2O_3 (○), Ga_2O_3/Al_2O_3(I) (▲), Ga_2O_3–Al_2O_3(S) (□), and Ga_2O_3 (◆) for NO oxidation into NO_2 in the absence of H_2O. Conditions: NO = 900 ppm, $O_2 = 10\%$, $H_2O = 0\%$, catalyst weight = 0.2 g, W/F = 0.18 g scm^{-3}.

TABLE 1

Physical Properties of Al_2O_3, Ga_2O_3/Al_2O_3(I), Ga_2O_3–Al_2O_3(S), and Ga_2O_3

Catalyst	BET surface area/ $m^2\ g^{-1}$	Mean pore size/nm	Pore volume/ $ml\ g^{-1}$
Al_2O_3	205	4.1	0.25
Ga_2O_3/Al_2O_3(I)	140	5.3	0.21
Ga_2O_3–Al_2O_3(S)	188	9.6	0.87
Ga_2O_3	18	8.1	0.06

Note: Mean pore size and pore volume were calculated using Dollimore–Heal (DH) theory from the desorption curve. Mean pore size represents pore radius, where the peak intensity in Fig. 4 is at a maximum. Pore volume is estimated in the region of pore radius less than 20 nm.

(42). A similar phenomenon might take place on the present catalysts.

3.2. *Catalyst Characterization*

In Table 1 are given the surface area, mean pore size, and pore volume of Al_2O_3, Ga_2O_3/Al_2O_3(I), Ga_2O_3–Al_2O_3(S), and Ga_2O_3. The pore size and pore volume distribution curves are shown in Fig. 6. The high surface area of Ga_2O_3–Al_2O_3(S) was comparable to that of Al_2O_3, while the surface area of Ga_2O_3/Al_2O_3(I) was much smaller than that of Al_2O_3 probably because of a blockage of the pores of Al_2O_3 by supported Ga_2O_3. In fact, an enlargement of the mean pore size and a decrease of the pore volume of Al_2O_3 were recognized after impregnation of gallium (Fig. 6b). As can be seen in Fig. 6c, Ga_2O_3–Al_2O_3(S) showed a broad pore size distribution curve with no distinct mean pore size, suggesting that no micro- and mesopores but only macropores are present. It was also found that Ga_2O_3–Al_2O_3(S) has a comparatively large pore volume. The BET surface area of Ga_2O_3 was found to be 18 $m^2\ g^{-1}$, which is very small compared with that of the other catalysts.

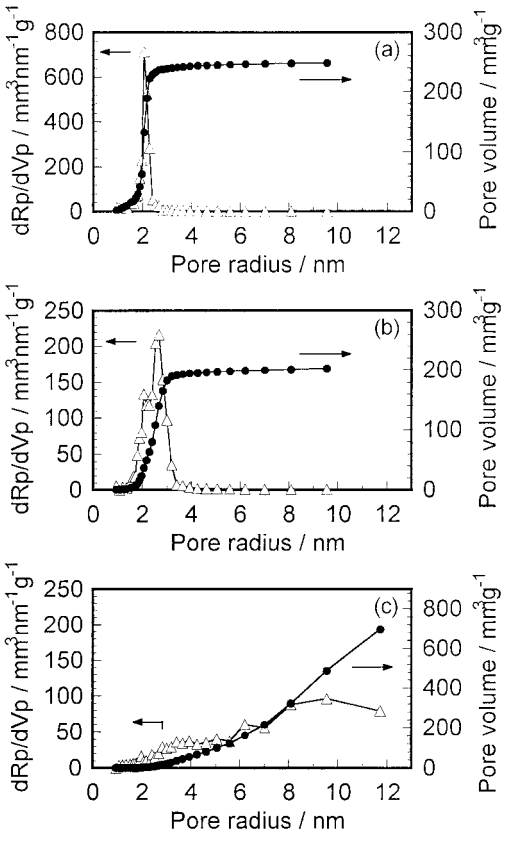

FIG. 6. Pore size distribution of (a) Al_2O_3, (b) Ga_2O_3/Al_2O_3(I), and (c) Ga_2O_3–Al_2O_3(S).

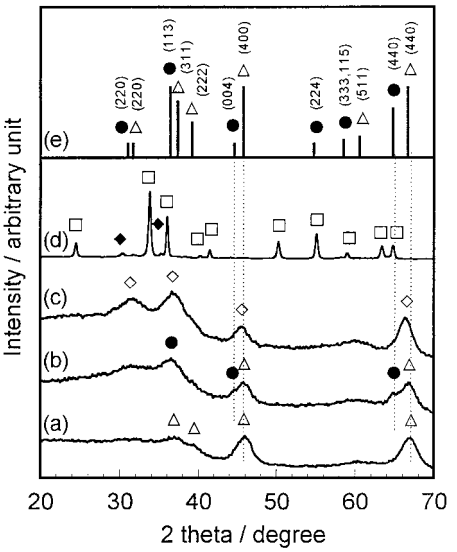

FIG. 7. XRD patterns of (a) Al_2O_3, (b) Ga_2O_3/Al_2O_3(I), (c) Ga_2O_3–Al_2O_3(S), (d) Ga_2O_3, and (e) γ-Al_2O_3 and γ-Ga_2O_3 from JCPDS data as reference (No. 10-425 and No. 20-426, respectively). (△) for γ-Al_2O_3, (●) for γ-Ga_2O_3, (□) for α-Ga_2O_3, (◆) for β-Ga_2O_3, and (◇) for solid solution (unidentified).

Figure 7 shows X-ray diffraction patterns of Al_2O_3, Ga_2O_3/Al_2O_3(I), Ga_2O_3–Al_2O_3(S), and Ga_2O_3. The crystallite structure of Al_2O_3 was γ-Al_2O_3. Two phases, α-Ga_2O_3 and β-Ga_2O_3, were detected for Ga_2O_3. Two kinds of XRD peaks assigned to γ-Al_2O_3 and γ-Ga_2O_3 were observed for Ga_2O_3/Al_2O_3(I), suggesting that Al_2O_3 and Ga_2O_3 are present independently. On the other hand, Ga_2O_3–Al_2O_3(S) showed an XRD pattern different from that of Ga_2O_3/Al_2O_3(I). Distinct peaks assigned to γ-Ga_2O_3 were not detected, but a shift of diffraction peaks at $2\theta = 45.5°$ and 66.5°, which can be assigned to respective γ-Al_2O_3(400) and −(440), toward lower angles was recognized, suggesting the formation of a solid solution of γ-Al_2O_3 and γ-Ga_2O_3.

SEM observation was performed for Ga_2O_3/Al_2O_3(I) and Ga_2O_3–Al_2O_3(S) to examine the texture of the catalyst surface. As depicted in Fig. 8a, the surface of Ga_2O_3/Al_2O_3(I) was very rough and the presence of pores was recognized. On the other hand, Ga_2O_3–Al_2O_3(S) showed a quite different surface morphology and seems to consist

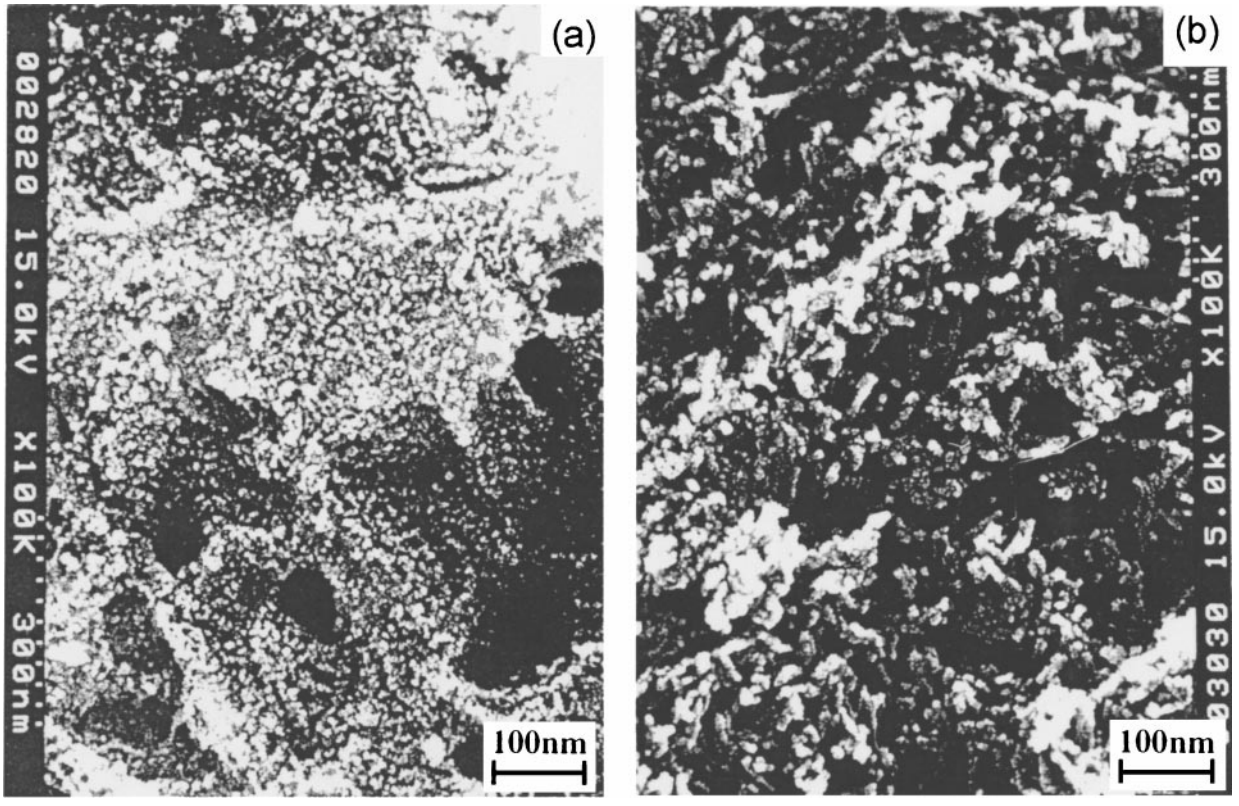

FIG. 8. SEM photographs of (a) Ga_2O_3/Al_2O_3(I) and (b) Ga_2O_3–Al_2O_3(S).

of fibrillar particles. Figure 9 shows TEM photographs of Ga_2O_3/Al_2O_3(I) and Ga_2O_3–Al_2O_3(S). In the photograph of Ga_2O_3/Al_2O_3(I) (Fig. 9a), a lot of nonuniform particles with the lattice spacing of ca. 0.25 nm, which can be assigned to γ-Ga_2O_3(113), were observed. The presence of distinct particles was not recognized in the photograph of Ga_2O_3–Al_2O_3(S). This might be because a solid solution of Al_2O_3 and Ga_2O_3 is formed as presumed from the XRD pattern. Interestingly, Ga_2O_3–Al_2O_3(S) was also found to consist of fibrillar particles from TEM observation.

We performed XPS measurements to reveal the electronic state of gallium species. XPS parameters obtained here are summarized in Table 2. The peak area ratio (Ga 2p/Al 2p) for Ga_2O_3/Al_2O_3(I) was higher than that for Ga_2O_3–Al_2O_3(S), suggesting that most of the Ga_2O_3 was deposited on the surface of Ga_2O_3/Al_2O_3(I). The binding energy of Ga 2p increased in the following order: $Ga_2O_3 < Ga_2O_3/Al_2O_3$(I) < Ga_2O_3–Al_2O_3(S). In Table 2 are also given the Auger parameters of gallium species. The concept of an Auger parameter, which is the sum of the binding energy of Ga 2p and the Auger kinetic energy of Ga (MNN), was proposed by Wagner *et al.* (43). The Auger parameter of gallium species decreased in the sequence of $Ga_2O_3 > Ga_2O_3/Al_2O_3$(I) > Ga_2O_3–Al_2O_3(S). The Auger parameters of a target element are known to be different depending upon the corresponding compound and the crystal structure (44). A difference in the chemical characteristics of gallium species such as the crystallite structure and the coordination number between Ga_2O_3/Al_2O_3(I) and Ga_2O_3-Al_2O_3(S) is also deduced from XPS measurements.

TABLE 2

Summary of Line Energies Obtained for Ga_2O_3, Ga_2O_3/Al_2O_3(I), and Ga_2O_3–Al_2O_3(S)

Catalyst	Peak area ratio Ga 2p/Al 2p	Binding energy of Ga 2p/eV	Auger kinetic energy of Ga(MNN)/eV	Auger parameter[a]/eV
Ga_2O_3	—	1118.10	1063.00	2181.10
Ga_2O_3/Al_2O_3(I)	0.189	1118.37	1061.99	2180.36
Ga_2O_3–Al_2O_3(S)	0.147	1118.53	1061.62	2180.15

[a] Auger parameters were estimated from the sum of binding energy of Ga 2p and Auger kinetic energy of Ga(MNN).

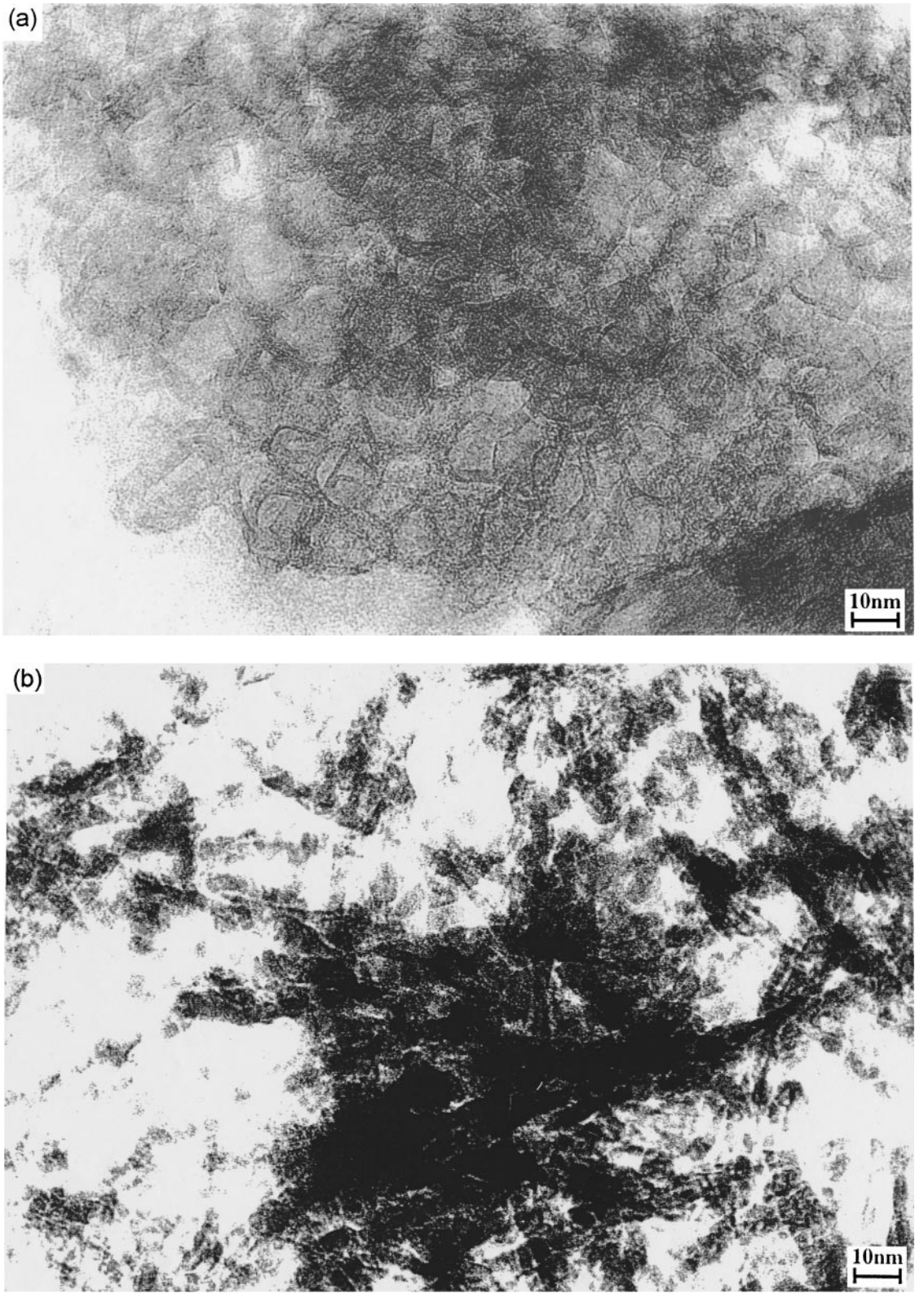

FIG. 9. TEM photographs of (a) Ga_2O_3/Al_2O_3(I) and (b) Ga_2O_3–Al_2O_3(S).

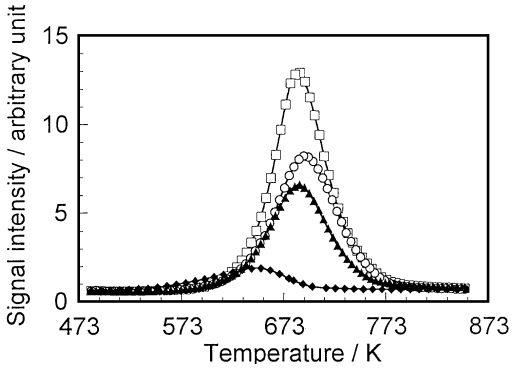

FIG. 10. TPD profiles of NO on Al_2O_3 (○), Ga_2O_3/Al_2O_3(I) (▲), Ga_2O_3–Al_2O_3(S) (□), and Ga_2O_3 (◆). The sample (50 mg) was pretreated in flowing 10% O_2/He at 873 K for 1 h, followed by NO adsorption in flowing 1000 ppm NO/10% O_2/He at room temperature for 2 h. TPD measurements were carried out up to 873 K with a heating rate of 5 K min^{-1} in flowing He (60 cm^3 min^{-1}).

3.3. NO TPD Studies

Figure 10 illustrates TPD profiles of NO on the catalysts prepared here. In this measurement, no desorption peaks ascribed to N_2O (mass number, 44) and NO_2 (mass number, 46) were observed. However, a desorption peak ascribed to O_2 (mass number, 32) from all the catalysts was observed simultaneously with desorption of NO. This fact suggests that nitrate species (NO_3^-) are formed on the catalyst surface during adsorption of NO + O_2 at room temperature and desorbed NO results from the decomposition of nitrates.

All the catalysts, Al_2O_3, Ga_2O_3/Al_2O_3(I), and Ga_2O_3–Al_2O_3(S), except for Ga_2O_3 showed similar TPD profiles in which the desorption peak of NO was centered around 690 K, as shown in Fig. 10. The desorption peak on Ga_2O_3 was observed at a relatively low temperature, 650 K, compared with those of the other catalysts. NO desorption from Ga_2O_3 was initiated at the lowest temperature. As summarized in Table 3, the amount of desorbed NO (μmol of NO g^{-1}) from the catalyst increased in the sequence Ga_2O_3 < Ga_2O_3/Al_2O_3(I) < Al_2O_3 < Ga_2O_3–Al_2O_3(S). The amounts of desorbed NO normalized by the BET surface area (μmol of NO m^{-2}) are also summarized in Table 3. Apparently,

TABLE 3

Summary of NO TPD Measurements

Catalyst	Temperature of NO desorption peak/K	Amount of desorbed NO	
		μmol of NO g^{-1}	μmol of NO m^{-2}
Al_2O_3	695	119.7	0.584
Ga_2O_3/Al_2O_3(I)	690	92.8	0.663
Ga_2O_3–Al_2O_3(S)	690	170.5	0.907
Ga_2O_3	650	24.7	1.372

TABLE 4

Summary of Kinetic Parameters of NO Reduction to N_2 by Propene at 723 K

Catalyst	Reaction order[a] with respect to			Activation energy[b]/ kJ mol^{-1}
	NO	C_3H_6	O_2	
Al_2O_3	0.3	0.3	0.6	85
Ga_2O_3/Al_2O_3(I)	0.3	0.3	0.6	92
Ga_2O_3–Al_2O_3(S)	0.0	0.3	0.7	92
Ga_2O_3	0.4	0.0	0.5	63

[a] Conditions: NO = 200–1500 ppm, C_3H_6 = 200–1500 ppm, O_2 = 3–10%, temperature = 723 K, gas flow rate = 66 cm^3 min^{-1}, catalyst weight = 0.03–0.08 g for Ga_2O_3/Al_2O_3(I), 0.01–0.03 g for Ga_2O_3–Al_2O_3(S), 0.1 g for Al_2O_3, 0.2 g for Ga_2O_3.

[b] Activation energies were calculated by varying the temperatures from 673 to 773 K under the following reaction conditions: NO = 900 ppm, C_3H_6 = 900 ppm, O_2 = 10%, H_2O = 0%, gas flow rate = 66 cm^3 min^{-1}.

Ga_2O_3 gave the highest value, suggesting that the adsorption site of NO on Ga_2O_3 is different from that on the other catalysts.

3.4. Kinetic Studies of NO Reduction by Propene over Ga_2O_3–Al_2O_3

The kinetic parameters and the activation energies for N_2 formation are summarized in Table 4, where the former was determined from ln–ln plots of the rate against the partial pressure of NO, C_3H_6, or O_2 and the latter from the Arrhenius plots. Good linear correlation was obtained within experimental error. Al_2O_3 and Ga_2O_3/Al_2O_3(I) gave similar kinetic parameters including activation energy. The rate equation is expressed as

$$r_{N_2} = kP_{NO}^{0.3,0.4}P_{C_3H_6}^{0.3}P_{O_2}^{0.6}\exp(-82000,\ -92000/RT). \quad [2]$$

A significant difference in the reaction order with respect to NO was recognized between Ga_2O_3/Al_2O_3(I) and Ga_2O_3–Al_2O_3(S), although the kinetic orders for C_3H_6 and O_2 as well as activation energy were almost the same. The reaction order with respect to NO on Ga_2O_3–Al_2O_3(S) was zero, suggesting that the catalyst surface is covered with NOx species, probably NO_3^- adspecies. The rate equation is as follows:

$$r_{N_2} = kP_{NO}^{0.0}P_{C_3H_6}^{0.3}P_{O_2}^{0.7}\exp(-92000/RT). \quad [3]$$

On the other hand, Ga_2O_3 gave a great different kinetic order with respect to C_3H_6, which is −0.1, leading to the presumption that C_3H_6 is adsorbed strongly on Ga_2O_3 and inhibits the N_2 formation. The rate equation is described by

$$r_{N_2} = kP_{NO}^{0.4}P_{C_3H_6}^{-0.1}P_{O_2}^{0.5}\exp(-63000/RT). \quad [4]$$

4. DISCUSSION

4.1. Relationship between Catalytic Performance and Physical Properties of Ga_2O_3–Al_2O_3

4.1.1. Activity of Ga_2O_3–Al_2O_3 for NO reduction by propene. As shown in Fig. 1, it was found that the catalytic performance of Ga_2O_3–Al_2O_3 for the selective reduction of NO with propene is quite dependent upon the catalyst preparation method even though the compositions are the same. Its tendency did not change in the presence of H_2O, although the activity was depressed by H_2O (Fig. 2). Apparently, Ga_2O_3–Al_2O_3(S) showed the highest catalytic activity of all the Ga_2O_3–Al_2O_3 catalysts.

The sol–gel technique is a useful method to prepare catalysts with highly dispersed species, compared to the impregnation method (21, 39, 45). It is also possible to prepare catalysts with interesting crystal structure by employing the sol–gel method (39). In the present study, the dispersion state and the crystal structure of gallium species of Ga_2O_3/Al_2O_3(I) are presumed to be different from those of Ga_2O_3–Al_2O_3(S). Therefore, we will discuss the difference of the catalytic performance, especially by focusing on the dispersion state and the crystal structure of gallium species, below.

4.1.2. Structural characterization of Ga_2O_3–Al_2O_3. (A) Physical properties. A great difference in the shapes of Ga_2O_3/Al_2O_3(I) and Ga_2O_3–Al_2O_3(S) was observed by SEM and TEM measurements. As depicted in Figs. 8 and 9, Ga_2O_3–Al_2O_3(S) was found to consist of a lot of fibrillar particles, while the presence of nonuniform particles was recognized in the photographs of Ga_2O_3/Al_2O_3(I). In addition, as can be seen in Fig. 6, the pore structure of Ga_2O_3–Al_2O_3(S) is different from that of Al_2O_3 and Ga_2O_3/Al_2O_3(I). A broad distribution curve was observed for the former catalyst and a sharp one centered around 4–5 nm for the latter two catalysts.

Since one of the features of the sol–gel method is to form M_1–O–M_2 bondings in the process of gelation (45), the formation of M_1–O–M_2 bondings is supposed to affect the pore structure and the particle shape. However, we reported that the pore structure of Co/Al_2O_3 (21) and CeO_2/Al_2O_3 (46) prepared by the same sol–gel method as the present work is almost the same as that of Al_2O_3 but obviously different from that of Ga_2O_3–Al_2O_3(S). Unique properties of Ga_2O_3–Al_2O_3(S) might result from the combination of the use of the sol–gel method and the similar properties of Ga_2O_3 and Al_2O_3. Ueno *et al.* (40, 41) reported that the alumina precursors produced by hydrolysis of AIP in hot water are composed of fibrillar pseudo-boehmite sols, where their length and thickness were estimated to be 40–80 and 8–10 nm, respectively, according to TEM observation. Since we employed almost the same method as that used by Ueno *et al.* for catalyst preparation in the present work, the same kind of aluminium boehmite sols should be formed. Since the crystal phase of alumina is similar to that of gallium oxide (47), the formation of Ga–O–Al bondings would be expected without changes in the shape of fibrillar pseudo-boehmite sols, resulting in the unique pore structure and particle shape of Ga_2O_3–Al_2O_3(S).

(B) Identification of crystal structure. Since several phases of gallium oxide, for example, α-, β-, γ-, δ-, and ε-Ga_2O_3 (47), closely resemble those of Al_2O_3, a substitution of Al ion and Ga ion at the interface of Al_2O_3 and Ga_2O_3 particles is expected. In fact, as shown in Fig. 7, a shift of X-ray diffraction peaks at $2\theta = 45.5^\circ$ and 66.5°, which can be assigned to respective γ-Al_2O_3(400) and $-$(440), toward lower angles was recognized for Ga_2O_3–Al_2O_3(S). This means that Ga ions are incorporated into the γ-Al_2O_3 lattice, namely, the formation of a solid solution, where the radius of the Ga^{3+} ion (0.062 nm) is larger than that of the Al^{3+} ion (0.051 nm). On the other hand, as for Ga_2O_3/Al_2O_3(I), the substitution of Ga ions with Al ions does not seem to occur, since γ-Ga_2O_3 and γ-Al_2O_3 are present independently.

In order to examine in detail the crystal structure of Ga_2O_3–Al_2O_3(S), changes in the XRD peak assigned to γ-Al_2O_3(440) and its lattice constant with Ga_2O_3 content (mol%) were measured. The results are shown in Fig. 11. The linear correlation was observed in the region of Ga_2O_3 content below ca. 27 mol% (40 wt%). It is noted that the diffraction peaks for Ga_2O_3–Al_2O_3(S) consist of single peaks without shoulder peaks and split peaks (Fig. 7c). Taking into account these results, we can consider that composite oxides such as $[Ga_xAl_{(1-x)}]_2O_3$ ($x < 1$) are formed uniformly in Ga_2O_3–Al_2O_3(S).

The structural differences between Ga_2O_3/Al_2O_3(I) and Ga_2O_3–Al_2O_3(S) might be also explained by the Auger parameters determined from XPS measurements. As can be seen in Table 2, the highest Auger parameter was obtained for Ga_2O_3 and the Auger parameter of gallium species

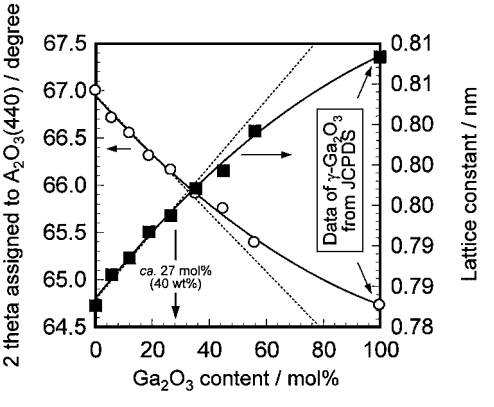

FIG. 11. Change in the peak position assigned to γ-Al_2O_3(440) (○) and the lattice constant of Al_2O_3 (■) in Ga_2O_3–Al_2O_3(S) with Ga_2O_3 loading.

is higher for Ga_2O_3/Al_2O_3(I) than for Ga_2O_3–Al_2O_3(S). Wagner *et al.* (44) measured the Auger parameters of aluminum species for several aluminum compounds, and revealed that their Auger parameter decreases in the sequence of $Al_2O_3 > SiO_2$–$Al_2O_3 >$ zeolites. This suggests that the more uniform a composite oxide is, the smaller the Auger parameter is. Therefore, gallium species in Ga_2O_3–Al_2O_3(S) are presumed to be dispersed more uniformly than those in Ga_2O_3/Al_2O_3(I).

Consequently, we can conclude that the difference in the crystal structure between Ga_2O_3/Al_2O_3(I) and Ga_2O_3–Al_2O_3(S) is as follows: (i) in Ga_2O_3/Al_2O_3(I), γ-Ga_2O_3 particles are dispersed on the surface of γ-Al_2O_3 and their particle size is relatively large, and (ii) in Ga_2O_3–Al_2O_3(S), a composite oxide such as $[Ga_xAl_{(1-x)}]_2O_3$ ($x < 1$) is formed uniformly in the catalyst.

4.1.3. Active sites of Ga_2O_3–Al_2O_3 for NO reduction by propene. In order to compare in detail the activities, we calculated reaction rate (μmol min^{-1} g^{-1}) and specific activity (nmol min^{-1} m^{-2}), normalized by BET surface area, for NO reduction to N_2 at 723 K. As summarized in Table 5, the specific activity of Al_2O_3 was increased by the presence of Ga_2O_3 irrespective of preparation method. Relatively high specific activity was obtained for Ga_2O_3 itself, suggesting that the presence of highly dispersed Ga_2O_3 is necessary to attain a high catalytic activity. Ga_2O_3–Al_2O_3(S) showed the highest specific activity.

Table 5 also shows two kinds of turnover frequency (TOF) for N_2 formation at 723 K. The TOF-NO and TOF-M were calculated on the basis of the amount of desorbed NO (Table 3) and the number of surface metal ions (Al or Ga), respectively. The number of surface Al and Ga ions on Al_2O_3 and Ga_2O_3 was estimated from the BET surface area combined with the theoretical surface density of Al (14.5 nm^{-2} for the (111) face of γ-Al_2O_3 (48)) and Ga (14.0 nm^{-2} for the (001) face of α-Ga_2O_3 (36)), respectively. Recently, Shimizu *et al.* (49) reported the equation concerning the relationship between the peak intensity ratio of I_{Ga}/I_{Al} evaluated by XPS and the coverage of Ga species on the surface of Al_2O_3. On the basis of their calculation method, the coverage of Ga species was estimated to be 0.452 and 0.357 for Ga_2O_3/Al_2O_3(I) and Ga_2O_3-Al_2O_3(S), respectively. The number of surface Ga ions was also calculated from the coverage of Ga species and the number of surface cation sites of Al_2O_3.

It was found that both the TOF-NO and the TOF-M show the same tendency, although the former TOF was much higher than the latter one. This is probably because NO is adsorbed not only on metal ions but also on the neighboring oxygen basic sites. As can be seen in Table 5, the turnover frequency of Al_2O_3 and Ga_2O_3 was much less than that of Ga_2O_3-Al_2O_3(S), indicating a synergistic effect between Ga_2O_3 and Al_2O_3. The TOF-NO and TOF-M of Ga_2O_3-Al_2O_3(S) are higher than those of Ga_2O_3/Al_2O_3(I) by a factor of about 1.5 and 3.6, respectively. The difference in the crystal structures of Ga_2O_3/Al_2O_3(I) and Ga_2O_3-Al_2O_3(S) seems to be responsible for the difference in the specific activity and the turnover frequency. It is noted that the turnover frequency for Ga_2O_3 is almost the same as that for Ga_2O_3/Al_2O_3(I). Shimizu *et al.* (36, 49) reported that the local structure of Ga atoms, GaO_4 tetrahedra highly dispersed in the surface spinel, is very important to determine the catalytic activity of Ga_2O_3/Al_2O_3 for NO reduction by methane. In the case of Ga_2O_3/Al_2O_3(I), similar reaction sites for NO reduction by propene would be possible. Namely, the gallium species dispersed on the surface is the reaction sites for Ga_2O_3/Al_2O_3(I). On the other hand, in the case of Ga_2O_3–Al_2O_3(S), new reaction sites created by a synergistic effect between Ga and Al ions (represented by "Ga–Al sites") in a composite oxide $[Ga_xAl_{(1-x)}]_2O_3$ ($x < 1$) would be proposed.

4.2. Proposed Reaction Mechanism

The selective reduction of NO with hydrocarbons is a very complex reaction comprising several parallel and/or consecutive reaction steps. As for the initial step of this

TABLE 5

Reaction Rates, Specific Activities, and Turnover Frequencies (TOF) of Al_2O_3, Ga_2O_3/Al_2O_3(I), Ga_2O_3–Al_2O_3(S), and Ga_2O_3 for NO Reduction to N_2 by Propene in the Absence of H_2O at 723 K[a]

Catalyst	Number of surface Al and Ga ions/mmol g^{-1}	Reaction rate/ μmol min^{-1} g^{-1}	Specific activity/ nmol min^{-1} m^{-2}	TOF-NO[d]/ $\times 10^{-2}$ min^{-1}	TOF-M[e]/ $\times 10^{-3}$ min^{-1}
Al_2O_3	4.94[b]	3.04	14.8	2.54	0.62
Ga_2O_3/Al_2O_3(I)	1.56[c]	6.61	47.2	7.12	4.23
Ga_2O_3–Al_2O_3(S)	1.23[c]	18.6	98.9	10.9	15.1
Ga_2O_3	0.42[c]	1.75	97.2	7.09	4.18

[a] Reaction conditions: NO = 900 ppm, C_3H_6 = 900 ppm, O_2 = 10%, H_2O = 0%, temperature = 723 K, gas flow rate = 66 cm^3 min^{-1}.
[b] Number of surface Al ions.
[c] Number of surface Ga ions.
[d] The TOF-NO was calculated on the basis of the amount of desorbed NO (Table 3).
[e] The TOF-M was calculated on the basis of the number of surface metal ions (Al or Ga).

reaction, many discussions have been published so far. In many cases, NO reduction by hydrocarbons is believed to proceed through reaction of hydrocarbons with NO_2, which is produced by oxidation of NO by oxygen (3, 8, 10, 22, 33, 50, 51). In this study, it was found from the comparison of the reactivity between NO and NO_2 that the reactivity of NO_2 is much higher than that of NO and that propene conversion is enhanced considerably by using NO_2 instead of NO (Fig. 4). These findings suggest the participation of NO_2 in NO reduction. On the other hand, Al_2O_3, Ga_2O_3/Al_2O_3(I), and Ga_2O_3 did not show activity for NO oxidation into NO_2 (Fig. 5), whereas these three catalysts were effective for NOx reduction into N_2 (Figs. 1 and 4). This result contradicts the reaction pathway proposed so far, in which NO oxidation to NO_2 is the initial and indispensable step for NO reduction by hydrocarbons.

Takeda and Iwamoto (52) reported the following rate equation for N_2 formation in the $NO + O_2 + C_2H_4$ reaction over Al_2O_3:

$$r_{N_2} = kP_{NO}^{1.1}P_{C_2H_4}^{0.1}P_{O_2}^{0.5}\exp(-294000/RT). \quad [4]$$

They proposed by comparing the rate equations obtained for $NO + O_2 + C_2H_4$ and $NO_2 + O_2 + C_2H_4$ reactions that the formation of NO_2 is the key step on Al_2O_3. On the other hand, in the present study, the reaction order with respect to NO was less than unity for all the catalysts tested here (Table 4). In particular, the reaction on Ga_2O_3–Al_2O_3(S) was found to proceed with zero-order kinetics for NO (Eq. [3]). These results suggest that the catalyst surface is covered with NOx adspecies such as nitrate species (NO_3^-). This is consistent with the results of NO TPD measurements (Fig. 10).

NOx adspecies, probably NO_3^-, formed on the catalyst surface is known to play an important role in NO reduction (53, 54). Meunier *et al.* (29) reported that the formation of organo-nitrite species followed by decomposition/oxidation but not the direct oxidation of NO with O_2 is the main route for the formation of NO_2 in NO reduction over Al_2O_3 and Ag/Al_2O_3. In the present study, the formation of NO_2 might proceed via similar reaction steps, although there is no evidence. Ga_2O_3–Al_2O_3(S) seems to promote effectively the formation of inorganic NOx adspecies, which is the precursor or organo-NOx compounds, as evidenced by NOx TPD measurements (Fig. 10).

It can be seen in Table 4 that the kinetic order with respect to C_3H_6 on Ga_2O_3/Al_2O_3(I) and Ga_2O_3–Al_2O_3(S) is 0.3, suggesting that C_3H_6 is adsorbed on the catalyst surface and then reacts with NOx and/or O_2 to form intermediates. Various organic compounds containing nitrogen and oxygen have been reported as candidates for the reaction intermediates based on organic chemistry literature. For example, Smits and Iwasawa (50) proposed the formation of the 1-nitro-*sec*-propyl radical by the reaction of NO_2 with oxygenated hydrocarbon (C_3H_6O). Adelman *et al.* (51) also reported that NO reduction by alkanes over Cu–ZSM-5 proceeds via the formation of 2-nitrosopropane by the reaction of NO with a *sec*-propyl radical formed by H-abstraction of alkane. Taking these reports into account, NO reduction by propene over Ga_2O_3–Al_2O_3 should proceed through the formation of organic compounds containing nitrogen and oxygen by the reaction of NO_2 formed via NOx adspecies with C_3H_6-derived species such as allyl species. Since propene conversion on Ga_2O_3–Al_2O_3(S) was much higher than that on Ga_2O_3/Al_2O_3(I) irrespective of NOx sources (NO or NO_2) (Figs. 1 and 4), the reaction of NO_2 with C_3H_6-derived species would be much faster on Ga_2O_3–Al_2O_3(S) than on Ga_2O_3/Al_2O_3(I). Finally, the resulting intermediate would be reduced to N_2 via several steps by the reaction with NOx and/or O_2.

5. CONCLUSIONS

Ga_2O_3–Al_2O_3 prepared by the sol–gel method (Ga_2O_3–Al_2O_3(S)) exhibited excellent activity for NO reduction by propene in the presence of oxygen, compared with Al_2O_3, Ga_2O_3, and Ga_2O_3/Al_2O_3 prepared by the impregnation method (Ga_2O_3/Al_2O_3(I)). The high catalytic activity of Ga_2O_3–Al_2O_3(S) was accounted for by the high surface area and the presence of $[Ga_xAl_{(1-x)}]_2O_3$ ($x < 1$) composite oxides. The formation of $[Ga_xAl_{(1-x)}]_2O_3$ ($x < 1$) composite oxides was presumed to result from supporting gallium species on the surface of aluminium boehmite needles as alumina precursor.

The reactivity of NO_2 was much higher than that of NO and propene conversion was enhanced considerably by using NO_2 instead of NO, suggesting the participation of NO_2 in NO reduction. On the other hand, direct oxidation of NO to NO_2 was found unimportant. A significant difference in the reaction order with respect to NO was recognized between Ga_2O_3/Al_2O_3(I) and Ga_2O_3–Al_2O_3(S), while the other kinetic parameters were almost the same. It should be noted that the reaction order with respect to NO was less than unity for all the catalysts, indicating that the catalyst surface is covered with NOx adspecies such as nitrate species (NO_3^-). From these findings, the formation of NOx adspecies, probably nitrates, was considered to be one of the important steps in NO reduction by propene over Ga_2O_3–Al_2O_3. The following reaction mechanism was suggested: NO_2 formed via NOx adspecies is reduced to N_2 through the formation of organic compounds containing nitrogen and oxygen by the reaction with propene-derived species.

REFERENCES

1. Shelef, M., *Chem. Rev.* **95**, 209 (1995).
2. Iwamoto, M., Mizuno, N., and Yahiro, H., *Sekiyu Gakkaishi* **34**, 375 (1991).

3. Hamada, H., Kintaichi, Y., Sasaki, M., Ito, T., and Tabata, M., *Appl. Catal.* **70**, L15 (1991).
4. Held, W., Koenig, A., Richter, T., and Puppe, L., *SAE Paper* 900496 (1990).
5. Iwamoto, M., Yahiro, H., Yu-u, Y., Sundo, S., and Mizuno, N., *Shokubai (Catalyst)* **32**, 430 (1990).
6. Ger. Offen. DE 3,642,018 (1987) to Volkswagen A.G.
7. Ger. Offen. DE 3,735,151 (1988) to Toyota Co.
8. Yokoyama, C., and Misono, M., *J. Catal.* **150**, 9 (1994).
9. Iwamoto, M., Yahiro, H., Shundo, S., Yu-u, Y., and Mizuno, N., *Appl. Catal.* **69**, L15 (1991).
10. Kikuchi, E., and Yogo, K., *Catal. Today* **22**, 73 (1996).
11. Tabata, T., Kokitsu, M., Ohtsuka, H., Okada, O., Sabatino, L. M. F., and Bellussi, G., *Catal. Today* **27**, 91 (1996).
12. Grinstedt, R. A., Jen, H.-W., Montreuil, C. N., Rokosz, M. J., and Shelef, M., *Zeolites* **13**, 602 (1993).
13. Keiski, R., Raisanen, H., Harkonen, M., Maunula, T., and Niemisto, P., *Catal. Today* **26**, 85 (1996).
14. Kintaichi, Y., Hamada, H., Tabata, M., Sasaki, M., and Ito, T., *Catal. Lett.* **6**, 239 (1990).
15. Teraoka, Y., Harada, T., Iwasaki, T., Ikeda, T., and Kagawa, S., *Chem. Lett.* 773 (1993).
16. Zhang, X., Walters, A. B., and Vannice, M. A., *J. Catal.* **155**, 290 (1995).
17. Okazaki, N., Shiina, Y., Itoh, H., Tada, A., and Iwamoto, M., *Catal. Lett.* **49**, 169 (1997).
18. Tabata, M., Hamada, H., Kintaichi, Y., Sasaki, M., and Ito, T., *Sekiyu Gakkaishi* **36**, 191 (1993).
19. Torikai, Y., Yahiro, H., Mizuno, N., and Iwamoto, M., *Catal. Lett.* **9**, 91 (1991).
20. Hamada, H., Kintaichi, Y., Sasaki, M., Ito, T., and Tabata, M., *Appl. Catal.* **75**, L1 (1991).
21. Nanba, T., Uemura, A., Ueno, A., Haneda, M., Hamada, H., Kakuta, N., Miura, H., Ohfune, H., and Udagawa, Y., *Bull. Chem. Soc. Jpn.* **71**, 2331 (1998).
22. Hamada, H., Kintaichi, Y., Inaba, M., Tabata, M., Yoshinari, T., and Tsuchida, H., *Catal. Today* **29**, 53 (1996).
23. Tabata, M., Hamada, H., Suganuma, F., Yoshinari, T., Tsuchida, H., Kintaichi, Y., Sasaki, M., and Ito, T., *Catal. Lett.* **25**, 55 (1994).
24. Haneda, M., Kintaichi, Y., Inaba, M., and Hamada, H., *Bull. Chem. Soc. Jpn.* **70**, 499 (1997).
25. Park, P. W., Kung, H. H., Kim, D.-W., and Kung, M. C., *J. Catal.* **184**, 440 (1999).
26. Yan, J. Y., Kung, M. C., Sachtler, W. M. H., and Kung, H. H., *J. Catal.* **172**, 178 (1997).
27. Bethke, K. A., and Kung, H. H., *J. Catal.* **172**, 93 (1997).
28. Bethke, K. A., Alt, D., and Kung, M. C., *Catal. Lett.* **25**, 37 (1994).
29. Meunier, F. C., Breen, J. P., Zuzaniuk, V., Olsson, M., and Ross, J. R. H., *J. Catal.* **187**, 493 (1999).
30. Miyadera, T., *Appl. Catal. B: Environ.* **2**, 199 (1993).
31. Miyadera, T., and Yoshida, K., *Chem. Lett.* 1483 (1993).
32. Aoyama, N., Yoshida, K., Abe, A., and Miyadera, T., *Catal. Lett.* **43**, 249 (1997).
33. Okazaki, N., Katoh, Y., Shiina, Y., Tada, A., and Iwamoto, M., *Chem. Lett.* 889 (1997).
34. Hoost, T. E., Kudla, R. J., Collins, K. M., and Chattha, M. S., *Appl. Catal. B: Environ.* **13**, 59 (1997).
35. Jen, H. W., *Catal. Today* **42**, 37 (1998).
36. Shimizu, K., Takamatsu, M., Nishi, K., Yoshida, H., Satsuma, A., and Hattori, T., *J. Chem. Soc., Chem. Commun.* 1827 (1996).
37. Shimizu, K., Satsuma, A., and Hattori, T., *Appl. Catal. B: Environ.* **16**, 319 (1998).
38. Haneda, M., Kintaichi, Y., Shimada, H., and Hamada, H., *Chem. Lett.* 181 (1998).
39. Haneda, M., Mizushima, T., Kakuta, N., Ueno, A., Sato, Y., Matsuura, S., Kasahara, K., and Sato, M., *Bull. Chem. Soc. Jpn.* **66**, 1279 (1993).
40. Ishiguro, K., Ishikawa, T., Kakuta, N., Ueno, A., Mitarai, Y., and Kamo, T., *J. Catal.* **123**, 523 (1990).
41. Ishikawa, T., Ohashi, R., Nakabayashi, H., Kakuta, N., Ueno, A., and Furuta, A., *J. Catal.* **134**, 87 (1992).
42. Yan, J. Y., Kung, H. H., Sachtler, W. M. H., and Kung, M. C., *J. Catal.* **175**, 294 (1998).
43. Wagner, C. D., Gale, L. H., and Raymond, R. H., *Anal. Chem.* **51**, 466 (1979).
44. Wagner, C. D., Six, H. A., Jansen, W. T., and Tayler, J. A., *Appl. Surf. Sci.* **9**, 203 (1981).
45. Ueno, A., Suzuki, H., and Kotera, Y., *J. Chem. Soc., Faraday Trans. 1* **79**, 127 (1983).
46. Haneda, M., Ph.D. Thesis, Toyohashi University of Technology, Japan, 1995.
47. Roy, R., Hill, V. G., and Osborn, E. F., *J. Am. Chem. Soc.* **74**, 719 (1952).
48. Knozinger, H., and Ratnasamy, P., *Catal. Rev. Sci. Eng.* **17**, 31 (1978).
49. Shimizu, K., Takamatsu, M., Nishi, K., Yoshida, H., Satsuma, A., Tanaka, T., Yoshida, S., and Hattori, T., *J. Phys. Chem. B* **103**, 1542 (1999).
50. Smits, R. H. H., and Iwasawa, Y., *Appl. Catal. B: Environ.* **6**, L201 (1995).
51. Adelman, B. J., Beutel, T., Lei, G.-D., and Sachtler, W. M. H., *Appl. Catal. B: Environ.* **11**, L1 (1996).
52. Takeda, H., and Iwamoto, M., *Bull. Chem. Soc. Jpn.* **69**, 2735 (1996).
53. Satsuma, A., Yamada, K., Sato, K., Shimizu, K., Hattori, T., and Murakami, Y., *Catal. Lett.* **45**, 267 (1997).
54. Shimizu, K., Kawabata, H., Satsuma, A., and Hattori, T., *J. Phys. Chem. B* **103**, 5240 (1999).